Int J Adv Manuf Technol (2016) 87:2731–2744
DOI 10.1007/s00170-016-8631-3

ORIGINAL ARTICLE

Research on modelling of ball-nosed end mill with chamfered cutting edge for 5-axis grinding

Wei Ji[1] · **Xianli Liu**[1] · **Lihui Wang**[2] · **Guangyue Wang**[1]

Received: 6 December 2015 / Accepted: 15 March 2016 / Published online: 2 April 2016

Abstract This paper presents models related to the manufacturing of ball-nosed end mills of solid carbide (BEMSC) with a chamfered cutting edge (CCE). A parallel grinding wheel (PGW) is selected, and the relationship between CCE face and PGW working face is determined. Based on the geometry models of BEMSC established in our previous work, the centre and axis vectors of PGW are calculated for the grinding of CCE face on bath the ball-nosed end and the cylinder, which is validated through a numerical simulation. In order to produce the tool, a grinding machine, SAACKE UMIF, is chosen. Targeting the grinding data of BEMSC, the transformations are carried out between the coordinate systems of workpiece and the NC programme according to the structural features of the machine. An algorithm is derived for dispersing grinding paths. As a result, the centre data and axis vector are generated with respect to the grinding machine. The BEMSC with CCE is machined using the selected machine, which demonstrates the correctness of the established models. Finally, the performance of the machined cutting tool is validated in comparison with a common BEMSC without CCE in the milling of a mould of a multi-hardness joint structure.

Keywords Ball-nosed end mill · Chamfered cutting edge · Parallel grinding wheel · Grinding path · Discretisation algorithm

✉ Wei Ji
weiji@hrbust.edu.cn; wei.ji@live.cn

[1] Harbin University of Science and Technology, Harbin 150080, China

[2] KTH Royal Institute of Technology, Stockholm 100 44, Sweden

Nomenclature

BEMSC	Ball-nosed end mill of solid carbide
CCE	Chamfered cutting edge
CR	Rake face
LF	Flank face
BEM	Ball-nosed end mill
BE	Ball end
PGW	Parallel grinding wheel
xyz	Coordinate frame of BEMSC
ω	Helix angle of cutting edge
θ	Angle between Z axis and $\vec{\mathbf{T}}$ in xyz
$\vec{T}$	Tangent vector of cutting edge at a certain value of φ, a parameter of cutting edge equation
xyz_1	Coordinate frame by rotating xyz around Z axis by η degree
η	Angle between X axis and the projection of $\vec{\mathbf{T}}$ in the plane of xoy in xyz
xyz_2	Coordinate frame by rotating xyz_1 around Y axis by θ degree
x_2oz_2	Plane in xyz_2
p_n	Normal plane at point P of cutting edge (x_2oy_2 of xyz_2)
p_{n0}	Normal plane at the joining point of ball-nosed end and helical groove cutting edges (p_n at the joining point)
p_s	Cutting plane perpendicular to the line between point P and the centre of the end ball
γ_n	Rake angle equivalent on p_n
γ_b	Chamfer angle equivalent on p_n
α_{n1}	First flank face angle on p_n
α_{n2}	Second flank face angle on p_n
$\omega_{n\alpha}$	Width of LF on p_{n0}
$\omega_{\gamma b}$	Width of CR at the intersection line of p_s and p_n on p_{n0}

$\omega_{\gamma n}$	Width of rake face at the intersection line of p_s and p_n on p_{n0}
l	Length from point P to Q on LF in xyz_2
ρ	Angle between OP and Y_2 axis in xyz_2
l_γ	Length from point Q to A on rake face in xyz_2
l_α	Length from point P to B on LF face in xyz_2
$\mathrm{xyz_{g2}}$	Coordinate frame by rotating xyz around X axis and Y axis
l_Δ	Distance between grinding wheel boundary and cutting edge on the cylinder in xyz_{g2}
$\vec{T}_{ww}$	Direction vector of grinding wheel axis in grinding of CCE on ball end
$\mathrm{l_g}$	Radius of grinding wheel
$\mathrm{w_g}$	Angle between grinding wheel and grinding face
$\vec{T}_{pw}$	Axis vector of grinding wheel in xyz for grinding of CCE on cylinder
$\vec{T}_{pw2}$	Axis vector of grinding wheel in xyz_{g2} for grinding of CCE on cylinder
xyz_p	Coordinate frame that SAACKE UWIF can recognise
A	Rotate angle of BEMSC around X axis
B	Swing angle of grinding wheel
ω_A	Rotate angle with positive x in xoz
xyz_{a2}	Coordinate system for grinding path discretisation
ε_g	Allowable grinding error

1 Introduction

Modern mould and die industry is characterised by high-efficiency machining requirement for the automotive industry, especially, for forming of car body panels. Most of semifinished moulds for example are treated by hardening before the finish machining process, and its hardness can be up to 50–65 HRC, which is a big challenge to the tool life of cutting tools. Ball-nosed end mills of solid carbide (BEMSC) is one of the cutting tools that are widely used to cut moulds and dies of freeform surfaces. When BEMSC is used in machining of dies steel with high hardness, the strength of its cutting edge is the main problem, resulting in such as chipping, mechanical fatigue cracking, and fracture. Therefore, proper design and manufacture of BEMSC is the key to the high performance of its cutting edge, in particular, the design and treatment of the cutting edge. The passivation treatment of the cutting edge is a main method; however, the accuracy of the cutting edge is difficult to control. Cutting edge generation by grinding is an alternative treatment, but it introduces another challenge due to the complexity of cutting edge curve. Targeting the manufacturing problem of cutting edge treatment by grinding, the objective of this research is to develop models of BEMSC with chamfered cutting edge (CCE) related to geometry design and manufacturing. The remainder of this paper is organised as follows. Section 2 reviews the state-of-the-art of the relevant research work about design and manufacturing of BEMSC. Section 3 introduces the modelling of BEMSC with CCE, of which the models of grinding path and position of wheel grinding are established in Section 4 and the models related to design and manufacturing of this kind of tools are verified by numerical simulation in MATLAB in Section 5. Section 6 introduces the process of grinding data generation after the selection of a grinding machine, SAACKE UWIF (http://www.saacke-group.com/scom/machines_model_uw1f.php). After BEMSC with CCE is machined, an evaluation of the experimental performance is carried out through the machining of a mould of a multi-hardness joint structure in Section 7. Finally, our research contributions are summarised in Section 8.

2 Literature review

Geometric design and NC machining are the keys for BEMSC with CCE. Most research has forced on these two topics.

2.1 Research on tool geometry

BEMSC consists of three parts: tool holder, helical groove (HG), and ball end (BE), as shown in Fig. 1. The tool holder is usually designed in several standard forms, e.g., straight holder and Morse taper holder. This research focuses on HG and BE, especially the cutting edge of the helical groove (CEHG) and the cutting edge of the ball end (CEBE). Regarding the helical angle (HA), two types of definitions exist: the angle between the cutting edge tangent line and the axis of tool revolution (HA1) [1], and the angle between the tangent of cutting edge line and the tangent of longitude line of ball (HA2) [2].

(1) Research on CEHG

CEHG is usually designed in different geometries, e.g., cone, ellipsoid, convex arc, and concave arc. Comprised with the common cylindrical HG, the CEHG modelling is the main target.

Cone: The cone HG of BEM is mainly used to avoid the interference with the workpiece during machining. The geometry modelling of cone HG was derived by Hsieh et al. [3], and that tool was manufactured in a 2-axis NC machine tool. Lai et al. [4] calculated the maximal sectional radius of

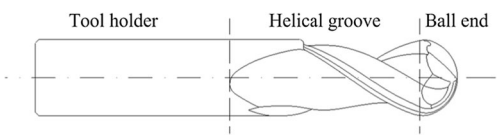

Fig. 1 A generic ball-nosed end mill structure

taper and the profile of the groove section as well as the feed rate of a grinding wheel under the definition of HA1. In order to avoid the instantaneous tilt angle of a grinding wheel, Bao et al. [5] defined the helical angle as a constant, which is the angle between its tool axis and the compound speed of the axial grinding speed of the wheel and the rotational velocity of a specific point on the cutting edge.

Convex arc: This type of tool is used to machine those workpieces with concave arc features. As Shang et al. [6] proposed, the cutting edge curve of BEMSC with elliptical outline was calculated by deriving the intersecting line between the elliptical cylinder and the rotational surface. The feed rate of a grinding wheel in the radial direction is modified according to the cross-section of the groove that passes through the centre of the cutter sphere under the definition of HA1. The shape of convex arc ball-nosed end mill is numerically approximated and produced by using a simple 2-axis NC machine. Wu et al. [7] presented the models of axial, rotary, and feeding velocity for the flute. Chen et al. [8] also proposed the models to calculate the actually obtained groove, and based on the models, a compensatory machining process was carried out to eliminate the residual profile of a cutting tool.

Concave arc: This type of tool is used to machine the workpieces with convex arc features. The cutting edge model on concave arc HG is derived by Chen et al. [9]. In compliance with the maximal sectional radius of a mill, the profile of the groove section as well as both the radial and axial cutting speeds of a chosen grinding wheel is computed.

(2) Research on CEBE

It is well known that the curves of CEBE are deemed to be the intersection of tool profile and helicoid. Obviously, the CEBE tool profile of BEMSC is a semisphere, and its equation is shown as follows:

$$r = \left\{ \sqrt{R^2 - z^2}\cos\phi, \sqrt{R^2 - z^2}\sin\phi, z \right\}, \quad 0 \le z \le R,\ 0 \le \phi \le 2\pi \quad (1)$$

where R, z, and ϕ are, respectively, the radius of semisphere, radius, and angle parameters.

Yuan et al. [10] demonstrated that the surface of a helicoid has two different definitions, a constant pitch and a constant helical angle. The following equation shows the condition of CEBE with a constant pitch. This type of tool is commonly used due to its fine machinability.

$$d\phi = \frac{RT}{2\pi\sqrt{\left(R^2 - z^2\right)^3}} \quad (2)$$

where T is the pitch of a helicoid surface.

Based on the models above, Chen and Lin [11] introduced a generic and integrated model for manufacturing the BEMSC with constant pitch helical grooves.

CEBE with a constant helical angle based on the definitions of HA1 and HA2 is shown in the following two equations, respectively [12]:

$$\phi = \frac{1}{2}\tan\beta \ln\frac{R+z}{R-z} \quad (3)$$

where β is the angle under HA1;

$$\phi = \int_0^Z \frac{\sqrt{R^2\tan^2\beta' - z^2\sec^2\beta'}}{R^2 - z^2} dz \quad (4)$$

where β' is the angle under HA2.

The same problem of the two curves is that the tip point of the tool is of no significance. During its production, the cutting edge is made with the curve of the constant helical angle far away from the tip point and another kind of curve near the tool tip [8]. Chen [13] used a spiral curve with constant pitch in the area of BE.

2.2 Research on NC grinding of BEM

Grinding path generation, grinding wheel positioning, and tracing play key roles in the manufacturing of BEMSC with CCE. Based on the tool geometrise and the grinding wheel used, the calculation approaches for grinding path generation can be classified into two categories: reverse calculation and forward calculation. The reverse calculation is to obtain the outline and profile of a nonstandard grinding wheel based on the movement of a given grinding machine and cutting tool geometries, whereas the forward calculation is to generate the grinding path based on the tool geometries after the selection of a standard grinding wheel.

(1) Reverse calculation

In this category, nonstandard grinding wheels are used, and the outlines and profiles of the grinding wheels are established based on the tool geometries and the grinding machine parameters. Research on manufacturing of three kinds of CEHG on BEM was carried out, e.g., general BEM, truncated-cone BEM (TCBEM), and concave cone-end milling cutter. Tsai et al. [14] proposed models related to the manufacturing of BEM with a constant helix angle on a 2-axis grinding machine, where the cross-section model of a grinding wheel and the solution model of the actual helical groove surface were presented. Lin et al. [12] presented models related to the manufacturing of BEM with a helical angle within the definition of HA2 using a 2-axis grinding machine, as

well as a compensatory grinding operation. Hsieh [3] presented a set of mathematical models for the design and manufacture of helical flute and cutting edge of TCBEM. The cross-section profile of a grinding wheel and the feed speed was deduced, which was validated by experiments carried out on a 2-axis grinding machine. Chen [15] also focused on manufacture of TCBEM, in which a supplementary cutting edge was designed towards the issue that there is no helical cutting edge on the top of BE. Chen et al. [16] proposed the modelling of concave cone-end milling cutter on a 2-axis grinding machine, where the cross-section profile, grinding path, and feed rate were provided for the grinding operation.

(2) Forward calculation

Forward calculation is usually used in multi-axis machining with standard grinding wheels. For BEM with a complex curved cutting edge, its grinding path is related to the translational motions (X, Y, and Z axes) and the rotational motions (A, B, and C) of machine tools. Different kinds of cutting tools have been studied. Feng and Hongzan [17] presented a new method of grinding path generation with a torus-shaped grinding wheel for grinding the rake face on tapered BEM, by which a constant rake angle can be obtained. Pham and Ko [18] reported a manufacturing model of flat end mill using a 5-axis grinding machine, and a prediction model of helical groove based on the given wheel profile and the relative movements between the cutting tool and the grinding wheel. As an advantage, the manufacturing cost is reduced. Rababah et al. [19] proposed a CNC grinding approach for the grinding of circular-arc BEM, including grinding wheel orientation and locations, and grinding path.

Many research works have focused on approaches for cutting tool grinding, such as grinding path generation and grinding wheel position determination. Karpuschewski et al. [20] introduced an automatic search approach for wheel positioning in flute grinding of cutting tools, of which the advantage is the reduction of material removal in the grinding wheel profiling operation. Chen and Bin [21] proposed a novel approach that utilises the self-adaptation features of a sphere to decrease the number of simultaneous cooperative axes of a CNC grinding tool, which can reduce the number of simultaneous movements from five to four and at the same time achieve a smooth transition of the rake face for grinding of tapered BEM. Chen et al. [22] presented the optimisation of the grinding process of an end mill of cemented tungsten carbide, including the approach and retract sequences of each axis and grinding parameters, resulting in up to 40 % improvement of machining efficiency. Kim et al. [23] proposed a method for design and manufacture of an end mill based on cutting simulation. The cutting tool model represents the tool geometry, grinding wheel geometry, and grinding path. Chen et al. [24] presented a new mathematical model and grinding approach of BEM, in which a conical wheel is employed to rake and flank faces to avoid interference. Nguyen and Ko [25] proposed a new model for determining the wheel position in grinding of BEM, where the rake face is generated by using the side face of the grinding wheel. Li et al. [26] reported a graphical analysis method to obtain the structural parameters and geometric shapes of helical grooves with the standard wheel geometry and position. They discussed the relationship between a helical groove and its grinding process. In comparison with the reverse calculation methods, the high-accuracy cutting geometry, such as flank face, rake face, and cutting edge, can be obtained via the forward calculations although 5-axis grinding machines are necessary.

From the literature survey, the reported works mainly studied the manufacturing related to the different types of BEMSC, rarely taking BEMSC with CCE into account. As Lu et al. [27] presented, cutting edge with chamfer in CR and land on LF has an advantage in the retentivity of cutting edge by experiments (see Fig. 2 for more details on LF and CR). However, how to manufacture the BEMSC with both LF and CR is unknown. Targeting this problem, this paper introduces a new modelling and grinding method for the cutting edge with LF and CR in the ball-nosed end of BEMSC and derives the needed paths and grinding wheel position for cutting edge grinding using the forward calculation approach. Also, the tool is machined by a SAACKE UWIF grinding machine, and the performance is validated by experiments.

3 Geometric modelling

3.1 Chamfered cutting edge modelling on BE

CCE is chosen as the cutting edge on BEMSC. Figure 2 illustrates the BE of BEMSC, including CR face, grinding path of

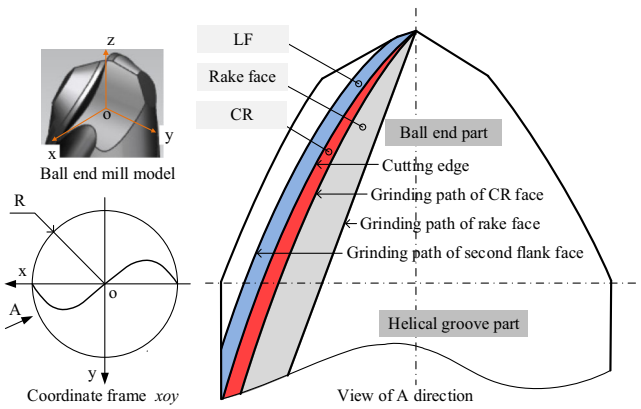

Fig. 2 An illustration of a ball-nosed end mill [28]

CR face, rake face, grinding path of rake face, LF face, and grinding path of the second flank face. As mentioned previously [28], the curve with a constant pitch is used as the cutting edge of BEMSC with CCE in order to increase the machinability of the cutting tool.

The curve of the cutting edge with a constant pitch can be expressed as follows:

$$\begin{cases} x = R\sqrt{1-(c\varphi)^2}\cos\varphi \\ y = R\sqrt{1-(c\varphi)^2}\sin\varphi \\ z = Rc\varphi \end{cases} \tag{5}$$

where $0 \le \varphi \le \tan\omega$.

The CR face is a complex 3D surface, and it is difficult to be modelled directly in xyz as most parameters are not defined in this coordinate system. Therefore, certain coordinate transformation must be applied. Figure 3 shows the transformations of coordinate systems of BEMSC, including xyz, $x_1y_1z_1$, and $x_2y_2z_2$. The tangent vector $\vec{\mathbf{T}}$ of the cutting edge can be calculated first by differentiating Eq. (6):

$$\vec{\boldsymbol{T}} = \begin{bmatrix} \dfrac{R(c^2\varphi^2\sin\varphi - c^2\varphi\cos\varphi - \sin\varphi)}{\sqrt{1-c^2\varphi^2}} \\ -\dfrac{R(c^2\varphi^2\cos\varphi + c^2\varphi\sin\varphi - \cos\varphi)}{\sqrt{1-c^2\varphi^2}} \\ cR \end{bmatrix}. \tag{6}$$

Based on the relationships among the three coordinate systems, the transformation matrix between xyz and $x_1y_1z_1$ can be determined, as well as that between xyz_1 and xyz_2. Finally, the relationship between xyz and $x_2y_2z_2$ is derived in Eq. (7).

$$\begin{bmatrix} x \\ y \\ z \end{bmatrix} = \boldsymbol{M}_{01}\boldsymbol{M}_{12}\begin{bmatrix} x_2 \\ y_2 \\ z_2 \end{bmatrix} \tag{7}$$

where

$$\mathbf{M}_{01} = \begin{bmatrix} \cos\eta & \sin\eta & 0 \\ -\sin\eta & \cos\eta & 0 \\ 0 & 0 & 1 \end{bmatrix}, \ \mathbf{M}_{12} = \begin{bmatrix} \cos\theta & 0 & -\sin\theta \\ 0 & 1 & 0 \\ \sin\theta & 0 & \cos\theta \end{bmatrix}.$$

$$\begin{cases} x_{Q2} = R\sqrt{1-(c\varphi)^2}\sin(\eta+\varphi) - l\cos\delta \\ y_{Q2} = Rc\varphi/\sin\theta + l\sin\delta \\ z_{Q2} = 0\,. \end{cases} \tag{8}$$

Finally, the coordinate of Q in xyz can be calculated by substituting Eq. (8) in Eq. (7):

$$\begin{bmatrix} x_Q \\ y_Q \\ z_Q \end{bmatrix} = \boldsymbol{M}_{01}\boldsymbol{M}_{12}\begin{bmatrix} x_{Q2} \\ y_{Q2} \\ z_{Q2} \end{bmatrix}. \tag{9}$$

The main challenge when calculating the grinding path of CR face is how to determine the relationship between the two parameters, l and φ. The boundary condition of l and φ is treated as the area between the l axis, φ axis, and the two dotted lines (AB and BC) in Fig. 4. The area can be

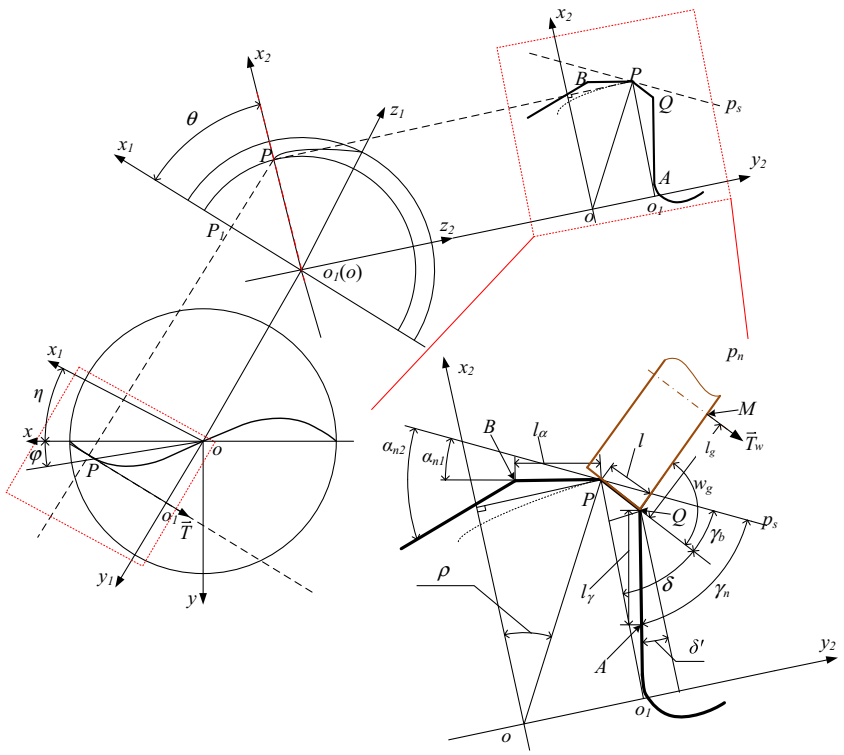

Fig. 3 Transformations of coordinate systems of BEMSC [28]

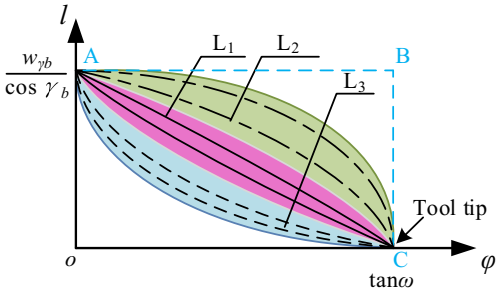

Fig. 4 Relationship between l and φ [28]

divided into three parts, denoted by L_1, L_2, and L_3, respectively. The lines in L_1 are close to a linear relationship. In other words, the fluctuation of $\omega_{\gamma b}$ is almost uniform from the tip to the joining point of BEMSC. As for the lines in L_2, the fluctuation of $\omega_{\gamma b}$ is significant near the tool tip and insignificant away from the tool tip. On the contrary, the lines in L_3 exhibit opposite trend as compared with the lines in L_2. Each line in L_1, L_2, and L_3 can be a single curve, e.g., straight line, hyperbola, parabola, ellipse, and may also be a set of piecewise curves.

In order to model the grinding path of the CR face, take a part of parabola with an upward opening in L_3 as an example. The point $(\tan\omega, 0)$ is chosen as the lowest point, and the curve passes a point $(0, \omega_{\gamma b}/\cos\gamma_b)$. Under this condition, the equation of the line can be determined by the following:

$$l = \frac{w_{\gamma b}}{\cos\gamma_b \cdot \tan^2\omega}(\varphi - \tan\omega)^2. \tag{10}$$

The grinding path of the CR face can then be derived by substituting Eq. (10) in Eq. (9).

3.2 Chamfered cutting edge on cylinder

The coordinate system (Fig. 2) is also selected for the CCE on cylinder, where the cutting edge curve on cylinder is defined as follows:

$$\begin{cases} x_g = R\cdot cos\left(-\varphi_g\right) \\ y_g = R\cdot sin\left(-\varphi_g\right) \\ z_g = -Rc\varphi_g \end{cases} \tag{11}$$

where φ_g is the parameter of the curve.

The tangent $\vec{\mathbf{T}}_{\mathbf{gt}}$ of the cutting edge is expressed as follows:

$$\begin{cases} x_{gt} = R\cdot sin\left(-\varphi_g\right) \\ y_{gt} = -R\cdot cos\left(-\varphi_g\right) \\ z_{gt} = -R\cdot c. \end{cases} \tag{12}$$

The modelling process is similar to CCE on BE. The transformation matrixes from xyz to xyz_{g2} are expressed as follows:

$$\begin{aligned} \boldsymbol{M}_{\boldsymbol{gz}}^{'} &= \begin{bmatrix} cos\left(-\theta_{gx}\right) & sin\left(-\theta_{gx}\right) & 0 \\ -sin\left(-\theta_{gx}\right) & cos\left(-\theta_{gx}\right) & 0 \\ 0 & 0 & 1 \end{bmatrix}, \boldsymbol{M}_{\boldsymbol{gy}}^{'} \\ &= \begin{bmatrix} cos\left(-\eta_{gz}\right) & 0 & -sin\left(-\eta_{gz}\right) \\ 0 & 1 & 0 \\ sin\left(-\eta_{gz}\right) & 0 & cos\left(-\eta_{gz}\right) \end{bmatrix} \end{aligned} \tag{13}$$

where θ_{gx} and η_{gz} are angle parameters related to the transformation of the coordinate systems.

Similarly, the transformation matrixes from xyz_{g2} to xyz are expressed as follows:

$$\begin{aligned} \boldsymbol{M}_{\boldsymbol{gy}} &= \begin{bmatrix} cos\,\eta_{gz} & 0 & -sin\,\eta_{gz} \\ 0 & 1 & 0 \\ sin\,\eta_{gz} & 0 & cos\,\eta_{gz} \end{bmatrix}, \boldsymbol{M}_{\boldsymbol{gz}} \\ &= \begin{bmatrix} cos\,\theta_{gx} & sin\,\theta_{gx} & 0 \\ -sin\,\theta_{gx} & cos\,\theta_{gx} & 0 \\ 0 & 0 & 1 \end{bmatrix}. \end{aligned} \tag{14}$$

In xyz_{g2}, as shown in Fig. 5, the chamfer on the cutting edge can be defined as follows:

$$\begin{cases} x_{gc2} = -\dfrac{\omega_{\gamma b} sin\left(\gamma_b - \phi_{px}\right)}{cos\,\gamma_b} \\ y_{gc2} = -\dfrac{\omega_{\gamma b}\, cos\left(\gamma_b - \phi_{px}\right)}{cos\,\gamma_b} \\ z_{gc2} = 0 \end{cases} \tag{15}$$

where ϕ_{px} and γ_b are two angles related to the chamfer parameters.

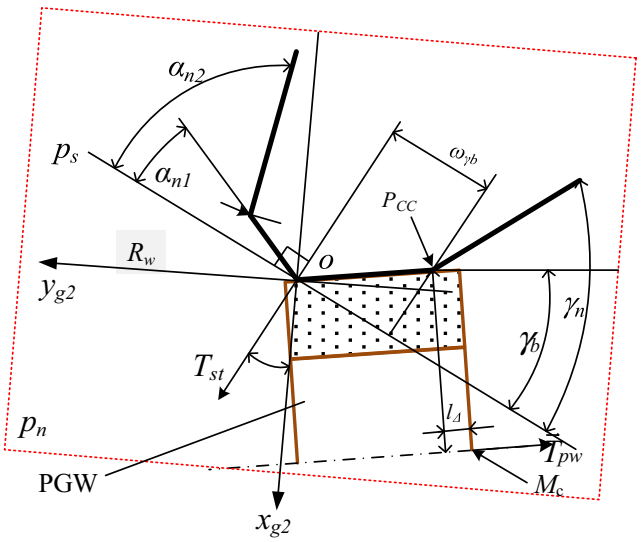

Fig. 5 Cross-section parameters of cutting edge on cylinder

Based on the transformation matrixes and Eq. (15), the coordinates of chamfer surface in *xyz* can be derived as follows:

$$\begin{bmatrix} x_{gc} \\ y_{gc} \\ z_{gc} \end{bmatrix} = \boldsymbol{M_{gz}M_{gy}} \begin{bmatrix} x_{gc2} \\ y_{gc2} \\ xz_{gc2} \end{bmatrix} + \begin{bmatrix} x_g \\ y_g \\ z_g \end{bmatrix}. \tag{16}$$

4 Grinding path generation

In order to machine the CCE of BEMSC, PGW is selected, and its cylindrical surface is used to grind the chamfer surface. The centre track and the position of PGW must be calculated first.

4.1 Grinding path modelling of CCE on BE

The centre path and the position are the keys. The relationship between the chamfer surface and PGW is determined first, as shown in Fig. 6. The *M* in xyz_2 can be calculated, as shown in Eq. (17).

$$\begin{cases} x_{m2} = x_{Q2} + l_g \sin\left(w_g + \delta - \pi/2\right) \\ y_{m2} = y_{Q2} + l_g \cos\left(w_g + \delta - \pi/2\right) \\ z_{m2} = z_{Q2} \end{cases} \tag{17}$$

where $w_g = \pi/2$ for PGW.

The grinding wheel position and the centre point of PGW can be determined by substituting Eq. (17) into Eq. (7).

Similarly, the direction vector $\vec{\mathbf{T}}_{\mathbf{ww}}$ of the grinding wheel axis in xyz_2 can be established as follows:

$$\begin{cases} x_{TW2} = \cos\left(3\pi/2 - w_g - \delta\right) \\ y_{TW2} = \sin\left(3\pi/2 - w_g - \delta\right) \\ z_{TW2} = 0. \end{cases} \tag{18}$$

The vector $\vec{\mathbf{T}}_{\mathbf{ww}}$ in xyz and the position of PGW can be determined by substituting Eq. (18) into Eq. (7).

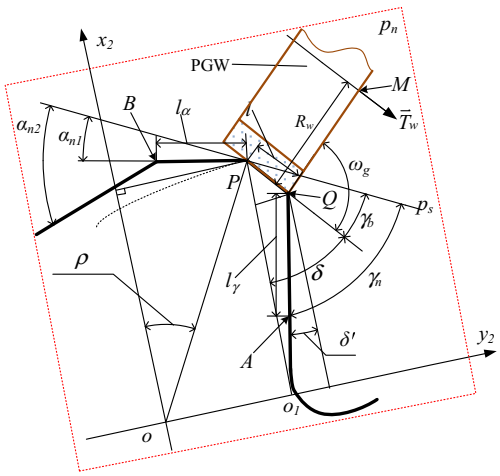

Fig. 6 Cross-section of cutting edge on ball end

4.2 Grinding path modelling for CCE on cylinder

Similarly, the centre path and position of PGW are calculated by the following procedure same as that of CCE on BE.

$$\begin{bmatrix} x_{Mc} \\ y_{Mc} \\ z_{Mc} \end{bmatrix} = \boldsymbol{M_{gz}M_{gy}} \begin{bmatrix} x_{Mc2} \\ y_{Mc2} \\ z_{Mc2} \end{bmatrix} + \begin{bmatrix} x_g \\ y_g \\ z_g \end{bmatrix}, \ where$$
$$\begin{cases} x_{Mc2} = x_{gc2} - l_\Delta \sin\left(\gamma_b - \phi_{px}\right) + R_g \cos\left(\gamma_b - \phi_{px}\right) \\ y_{Mc2} = y_{gc2} - l_\Delta \cos\left(\gamma_b - \phi_{px}\right) - R_g \sin\left(\gamma_b - \phi_{px}\right) \\ z_{Mc2} = 0 \end{cases} \tag{19}$$

where $(x_{Mc2}, y_{Mc2}, z_{Mc2})$ is the coordinate of the centre point in xyz_{g2}.

The axis vector $\vec{\mathbf{T}}_{\mathbf{pw}}$ of PGW is expressed as follows:

$$\vec{\boldsymbol{T}}_{\boldsymbol{pw}} = \boldsymbol{M_{gz}M_{gy}}\vec{\boldsymbol{T}}_{\boldsymbol{pw2}} + \begin{bmatrix} x_g \\ y_g \\ z_g \end{bmatrix}, \quad where \ \vec{\boldsymbol{T}}_{\boldsymbol{pw2}} = \begin{cases} x'_{gc2} = -\sin\left(\gamma_b - \phi_{px}\right) \\ y'_{gc2} = -\cos\left(\gamma_b - \phi_{px}\right) \\ z'_{gc2} = 0. \end{cases} \tag{20}$$

5 Numerical simulation

In order to validate all models related to the design and manufacturing of BEMSC with CCE, numerical simulations are carried out in MATLAB environment.

5.1 Simulation on geometry models

The geometries (size and angle) of the LF face, CR face, and rake face can be uniquely specified by γ_n, γ_b, α_{n1}, $\omega_{\alpha n}$, $\omega_{\gamma b}$, and $\omega_{\gamma n}$, respectively. Taking the CR face as an example with all the other parameters fixed, the results of the relevant models are depicted in Fig. 7. The cutting edges

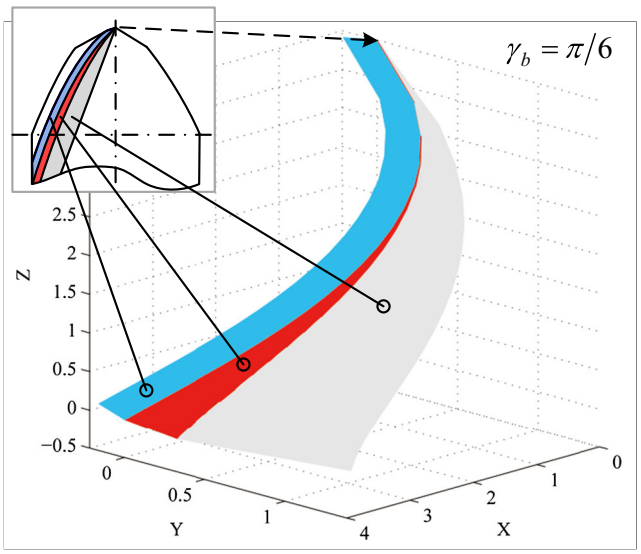

Fig. 7 Tool geometries of ball end in MATLAB simulation

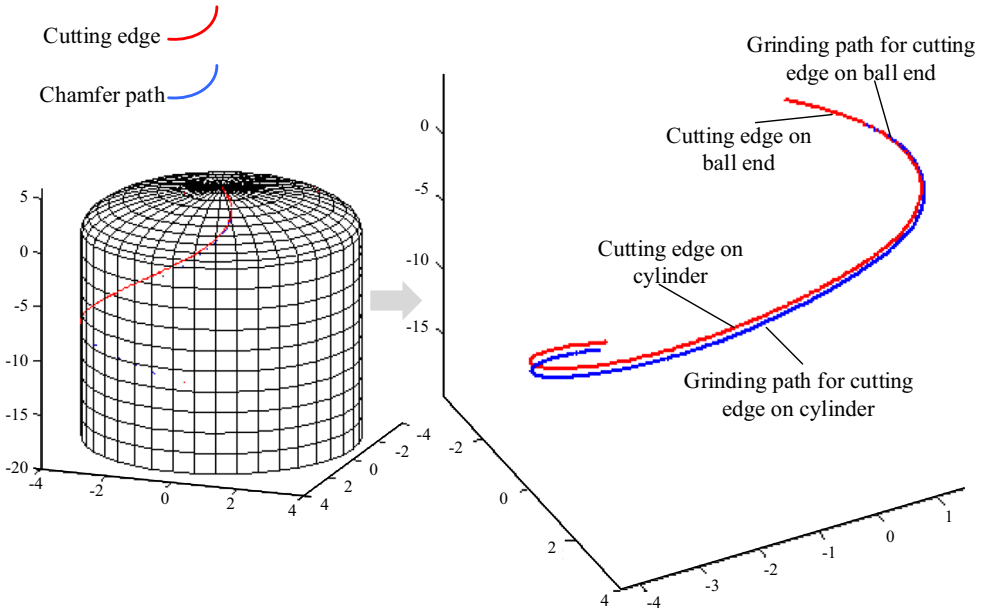

Fig. 8 Cutting edges on both ball end and cylinder in MATLAB simulation

on both BE and cylinder were simulated as well, as shown in Fig. 8, where the blue line represents the cutting edge, and red line indicates the grinding path for the grinding CCE.

5.2 Simulation of grinding path and wheel grinding

The centre and position of a grinding wheel are simulated for grinding of CEE both on BE and on cylinder. Figure 9 displays the simulation results of CEE on the BE, where the outline of PGW, the path and the axis vector of PGW centre, and the grinding path of chamfer are simulated. Similarly, Fig. 10 shows the simulation results of CEE on the cylinder.

From the simulation results, it is clear that the CCE of BEMSC can be machined by following the grinding path of PGW, which validates the correctness of the developed models. Hence, the grinding data can be generated based on our models.

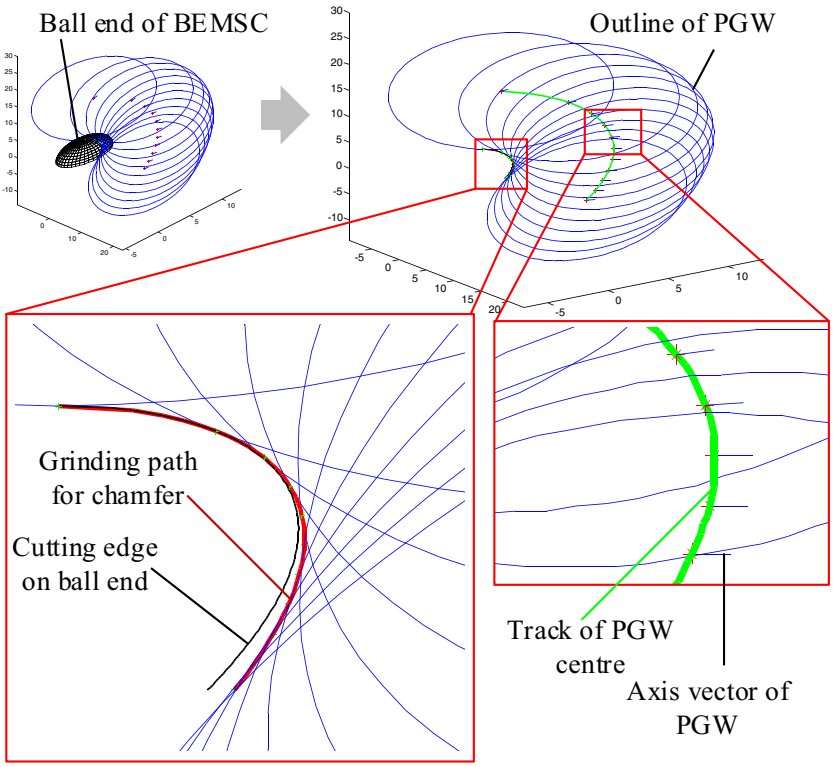

Fig. 9 Simulation on centre and position of grinding wheel in grinding of CCE on ball end

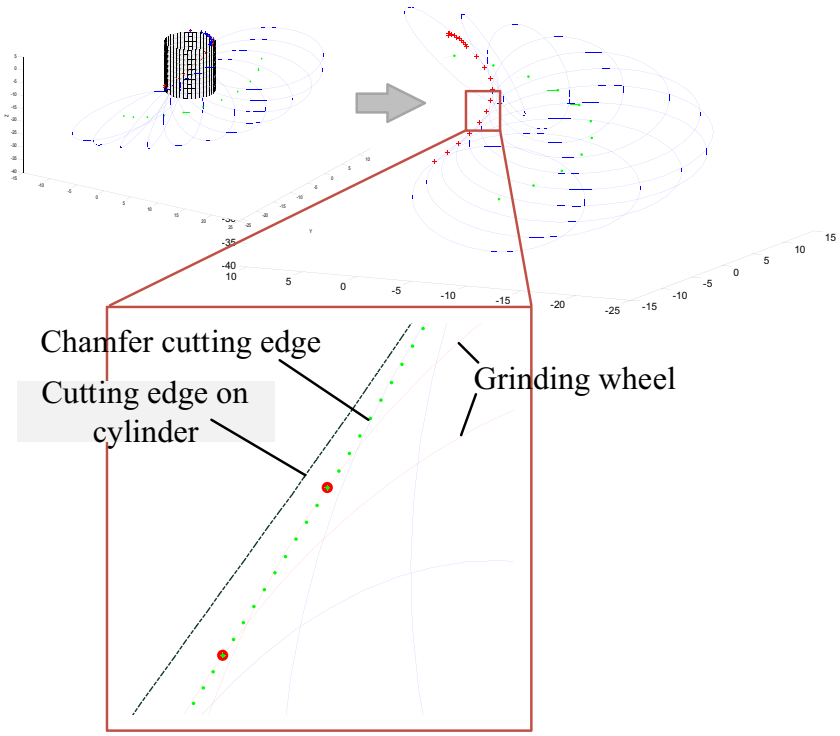

Fig. 10 Simulation on centre and position of grinding wheel in grinding of CCE on cylinder

6 Grinding data generation and simulation

The machining of BEMSC is carried out on a grinding machine, SAACKE UWIF, and its structure and possible movements are shown in Fig. 11. The grinding machine provides a useful function that NC code can be generated by inputting point data of a selected grinding wheel into the software embedded in the grinding machine. Therefore, the primary task is to transform the geometric data related to the manufacturing of BEMSC with CCE from the workpiece coordinate system (xyz) into the programming coordinate system (xyz_p) recognised by the software.

6.1 Transformation of coordinate systems

In xyz, BEMSC is fixed, and PGW can move around it, i.e., PGW has at least five degrees of freedom (DOF), *x*, y, z, A, and B. However, in xyz_p, BEMSC has three DOFs, x_p, y_p, and *A*, and PGW has only two DOFs, z_p and *B*. The transformation should be carried out to transform the grinding data from xyz to xyz_p. The transformation between the two coordinate systems is shown in Fig. 12, where the data file including the coordinates, x_p, y_p, z_p, *A*, and *B*, can be recognised by the SAACKE UWIF grinding machine. The DOF *A* of PGW can be removed by rotating BEMSC around its axis an angle, ω_A. *B* is related to the axis vector of PGW, and it is an angle A_{TW} between *y* axis

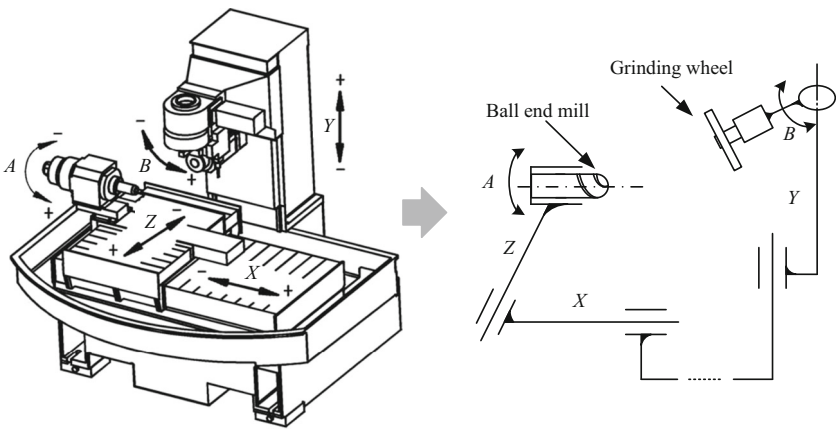

Fig. 11 Structure of SAACKE UWIF grinding machine and its movement model

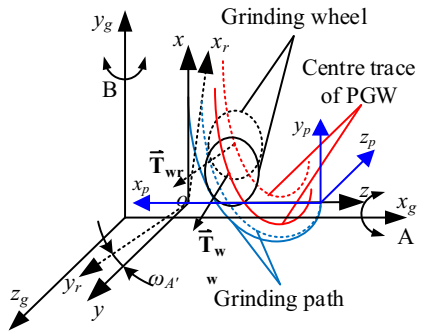

Fig. 12 Transformation between coordinate systems of workpiece and machine tool

and the projection of the rotated axis vector $\vec{\mathbf{T}}_{ww}$ on *yoz*. Therefore, based on the relationship between xyz and xyz_p, x_p, y_p, z_p, A, and B can be expressed as follows:

$$\begin{cases} x_p = R - x \\ y_p = \sqrt{x^2 + y^2}\cos\omega_A \\ z_p = \sqrt{x^2 + y^2}\sin\omega_A \\ A = \omega_A \\ B = A_{TW}. \end{cases} \tag{21}$$

6.2 Algorithm for discretisation of a continuous grinding path

The grinding machine, SAACKE UWIF, can only recognise the point data rather than curve equations. Therefore, the grinding point data must be detached from the continuous curve of BEMSC. As presented in [29], the curve discretisation methods include four types basically, e.g., equal spaced method, equal chord length method, equal error method (EEM), and feature points method. Here, the discretisation accuracy is determined by the selection of those methods. The accuracy of the equal spaced method is the lowest; accuracy of the equal chord length method is higher but the calculation is complex; the feature points method is not suitable due to the fact that no obvious feature points exist along the grinding path of BEMSC. Although the calculation process is complex, the accuracy of EEM is the highest. Therefore, EEM is chosen in this research.

Moreover, linear interpolation is used for grinding path discretisation in this paper. Based on the characteristics of EEM, the boundary condition is established first with respect to an allowable grinding error ε_g. Therefore, the cylinder of error boundary is more suitable. Figure 13a shows the cylinder in workpiece coordinate system xyz, where the direct error calculation is difficult in xyz. Therefore, the transformation is carried out from xyz to a new coordinate system that is suitable to computers. After rotating around x and z axes, respectively, the new system xyz_{a2} is obtained, as shown in

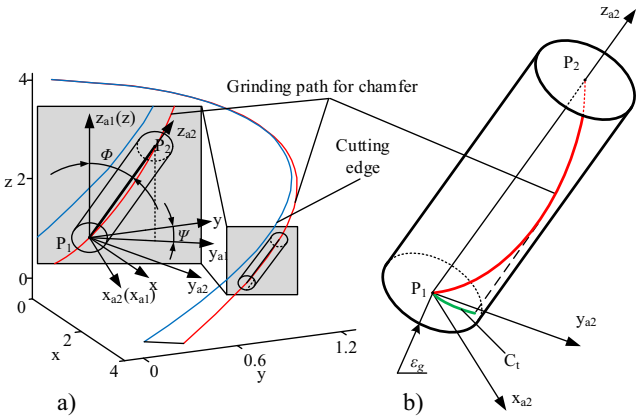

Fig. 13 Coordinate system transformation for grinding path discretisation

Fig. 13b. The discretisation condition can be derived, and the projection of the grinding path on the plane xoy_{a2} should be included within the circle of which the centre is P_1 and the radius is ε_g. Hence, the boundary condition can be expressed as follows:

$$\sqrt{x^2 + y^2} \le {\varepsilon_g}^2. \tag{22}$$

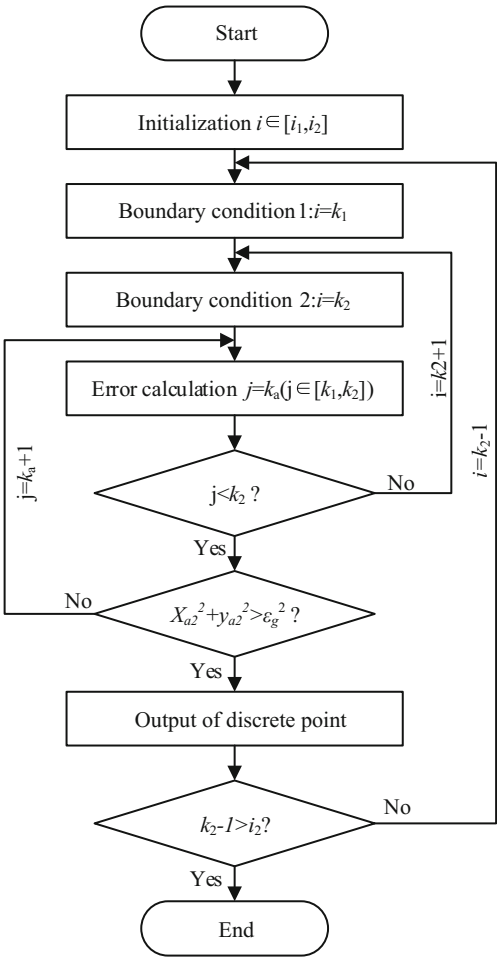

Fig. 14 Calculation process of grinding path discretisation

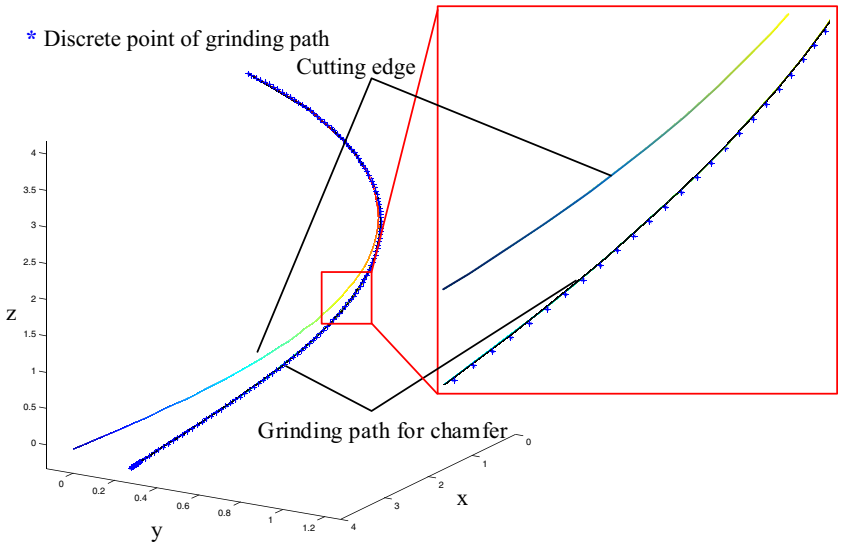

Fig. 15 Simulation results of grinding path coordinates against φ

The boundary condition provides the basis of judgement for discretising the grinding path.

6.3 Calculation of grinding point data

Based on the discretisation condition, the calculation of grinding point data follows the procedures depicted in Fig. 14, including initialising, setting boundary condition 1, setting boundary condition 2, calculating error, making two judgements based on the discretisation condition, generating grinding point data, and checking a termination condition.

Due to the complexity of the discretisation process, MATLAB software is used. The BEMSC parameters are pre-set as follows: $R = 4mm$, $\omega = \pi/6$, $\alpha_{n1} = \pi/18$, $\omega_{\alpha n} = 0.2mm$, $\omega_{\gamma b} = 0.3mm$, $\omega_{\gamma n} = 0.7mm$ and $\gamma_b = \pi/3$. The allowable error is $\varepsilon_g = 0.001\ mm$. The step size $\Delta\varphi$ is 0.0001 rad. According to the calculation procedures, the needed grinding data can be obtained. In order to validate the data, simulation is carried out in MATLAB environment. Figure 15 shows the simulation results of grinding path coordinates against φ. All of the points are on the grinding path, and their errors are within the allowable value, 0.001 mm.

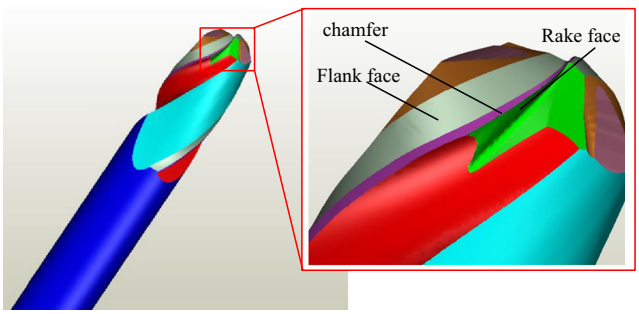

Fig. 16 Simulation result of grinding process

7 Experimental validation

In order to further validate the developed models of BEMSC, two grinding experiments have been carried out, including performance evaluation of BEMSC with CCE.

7.1 Grinding of BEMSC with CCE

A TXT file containing the grinding data obtained in Section 6.3 is downloaded to the SAACKE UWIF grinding machine. Considering the safety and security of the grinding machine, the grinding process of every feature was simulated before actual grinding, e.g., chamfer surface, rake face, and flank face. Figure 16 shows the results of the simulation,

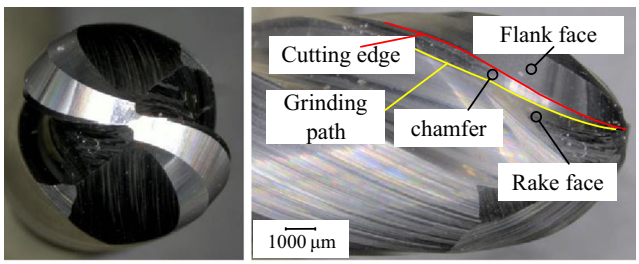

a) BEMSC with chamfered cutting edge

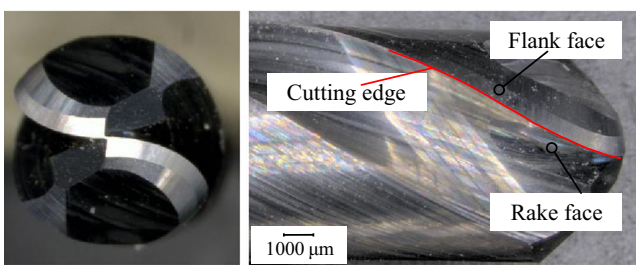

b) BEMSC without chamfer cutting edge

Fig. 17 Experimental results of two ball-nosed end mills

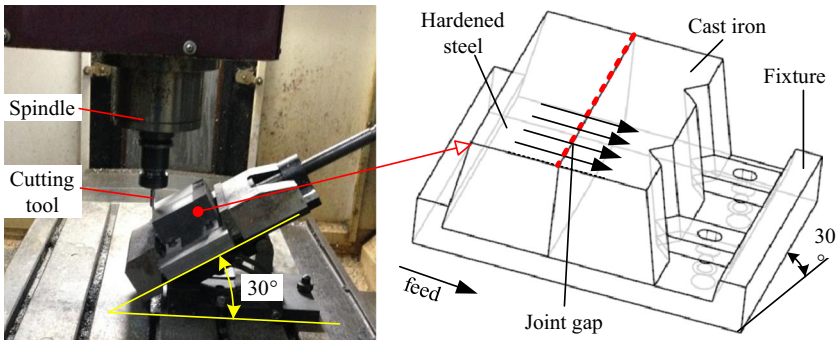

Fig. 18 Experimental setup of multi-hardness splitting workpiece

where the chamfer can be seen clearly. No collision and interference was found during the simulation.

After the safety checking through the simulation, the NC programme was executed in the real machine. The material of cutting tool is carbide GU25UF produced by Xiamen Golden Egret Special Alloy Co., LTD. Its grain size is 0.4 μm with 12 % cobalt content. The machined BEMSC with CCE is shown in Fig. 17a, whereas the BEMSC without CCE in Fig. 17b which is used for performance evaluation in Section 7.2. All the parameters of the two BEMSCs are the same except the chamfer.

7.2 Experimental evaluation on tool performance

A mould of multi-hardness joint structure was chosen as the workpiece to evaluate the tool performance. The mould is made of hardened steel and cast iron, of which the hardness are 55 and 42 HRC, respectively. The experimental setup is illustrated in Fig. 18. The cutting test was carried out on a Dalian VDL-1000E 3-axis machine tool without coolant. There is a 30° angle between the machined surface and the worktable of the machine tool. The feed direction is from the high hardness steel to the low hardness cast iron. The cutting parameters are cutting speed $v_c = 70$ m/min, cutting depth $a_p = 0.3$ mm, cutting width $a_e = 0.2$ mm, and feed rate $f = 0.15$ mm/z.

Theoretically, BEMSC with CCE has higher strength on cutting edge than BEMSC without CCE; however, the CCE may increase tool wear. Therefore, the condition of the cutting edge was observed and recorded every 20 min, and the wears of both tools are shown in Fig. 19, where Fig. 19a shows the tool wear start of BEMSC without CCE, Fig. 19b shows the

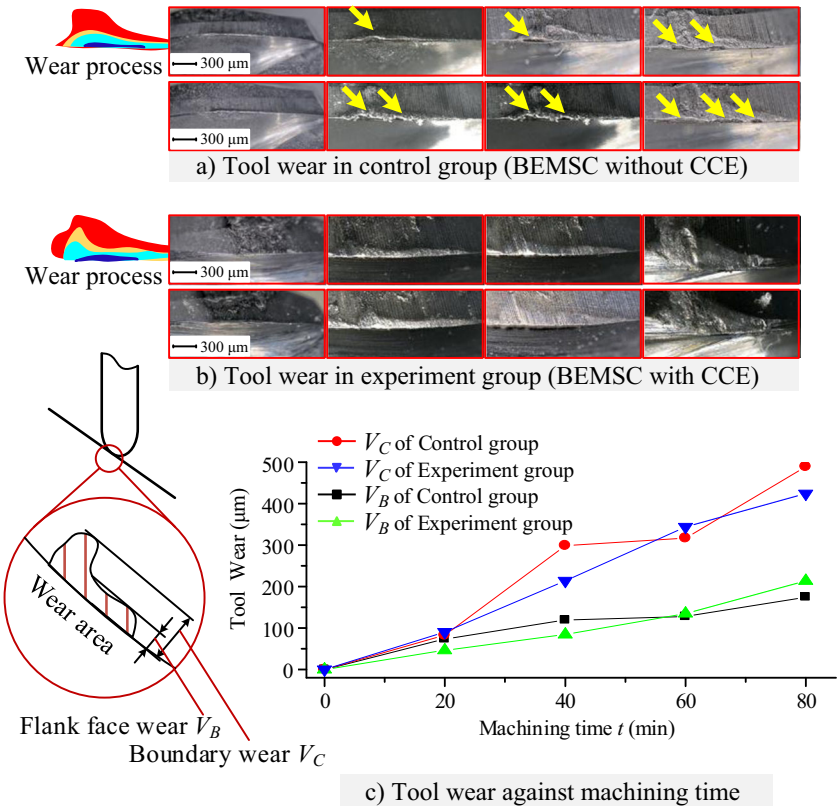

Fig. 19 Wear progression along cutting edges of two ball-nosed end mills

tool wear start of BEMSC with CCE, and Fig. 19c shows the progression of tool wear against machining time.

From Fig. 19a, b, it is visible that there is no chipping and fracture on the cutting edges of both tools during the first 20 min; after 40 min, chipping appeared on the tool without CCE; the number of chipping and fracture increased, and the areas of chipping and fracture became larger after 60 and 80 min, respectively. No chipping was observed on the tool with CCE.

Considering that the CCE may increase the cutting force and cutting temperature, one may argue that the CCE may also contribute to the tool wear. Therefore, in order to validate whether CCE affects the tool wear, wear values on the flank face were measured for the both tools. Figure 19c shows the wear curve of flank face wear on both the boundary and the main area, V_C and V_B. Boundary wear V_C is bigger than the main area wear V_B on both tools. According to the figure, tool wear values, V_C and V_B, on the two positions are almost the same, which highlights that CCE does not increase the tool wear.

The results of the two experiments indicate that the performance of the BEMSC with CCE is better than the tool without CCE, especially on the fracture resistance on the cutting edge. This validates our proposed method on modelling and grinding of BEMSC with CCE.

8 Conclusions

Targeting the manufacturing and performance evaluation of BEMSC with CCE, this paper presented a new method for grinding the CCE of BEMSC. Within the context, PGW is used together with our new geometry models, and the grinding path of the grinding wheel and grinding data are also generated. Numerical simulation and experiments are carried out to validate this approach. The uniqueness of this work can be summarised as follows:

(1) The position and path of the grinding wheel used in the grinding of BEMSC with CCE are calculated in two steps: determination of the interface relationship between PGW and chamfered face, and coordinate systems transformation. This approach offers an effective solution to chamfer machining for solid cutting tools with a complex cutting edge.

(2) NC programme can be generated easily through the transformation between the workpiece and the programming coordinate systems and the discretisation of a grinding path. The discretisation algorithm based on the equal error method is derived by establishing the error coordinate system and boundary condition. The algorithm can provide a way to obtain the dispersed grinding point data for a solid cutting tool.

(3) The BEMSC with CCE can be machined based on the models related to grinding of the cutting tool. In comparison with a common cutting edge, the CCE possesses better fracture resistance according to the experimental results. The chamfer is one type of effective cutting edge for the machining of high hardness materials.

Control of grinding accuracy is complex, and it depends on the grinding tool and grinding wheel. Therefore, our further research will focus on the models regarding the movement error compensation of grinding machines and the wear compensation of grinding wheels towards the high accuracy grinding of BEMSC with CCE.

Acknowledgments This project is supported by the National Natural Science Foundation of China (Grant No. 51235003).

References

1. Kaldor S, Rafael AM, Messinger D (1988) On the CAD of profiles for cutters and helical flutes—geometrical aspects. CIRP Ann Manuf Technol 37(1):53–56. doi:10.1016/S0007-8506(07)61584-4
2. Wu DR (1977) Course for differential geometry. People Education Press, Beijing
3. Hsieh JM (2006) Manufacturing models for design and NC grinding of truncated-cone ball-end cutters. Int J Adv Manuf Technol 35(11–12):1124–1135. doi:10.1007/s00170-006-0794-x
4. Lai HY, Chen WF (2002) Precision design and numerical control machining of tapered ball-end milling cutters. Proc Inst Mech Eng B J Eng Manuf 216(2):183–197. doi:10.1243/0954405021519834
5. Bao QS, Wang YT, Tang YY (2002) A new cutting edge of the conical ball-nosed milling cutter. J Hebei Univ Sci Technol 23(2): 40–42
6. Shang QH, Sun CH, Tang YY, Liu HM (2001) Study on geometrical modeling for elliptical edge of ball-end milling cutters. Tool Eng 35(5):7–8
7. Wu CT, Chen CK (2001) Manufacturing models for the design and NC grinding of a revolving tool with a circular arc generatrix. J Mater Process Technol 116:114–123
8. Chen WY, Chang PC, Liaw SD, Chen WF (2005) A study of design and manufacturing models for circular-arc ball-end milling cutters. J Mater Process Technol 161(3):467–477. doi:10.1016/j.jmatprotec.2004.07.086
9. Chen WF, Lai HY, Chen CK (2002) Design and NC machining of concave-arc ball-end milling cutters. Int J Adv Manuf Technol 20: 169–179
10. Yuan JP, Yu YT (2002) Virtual manufacturing models for 2-axis NC machining of ball-end milling cutters. Tool Eng 36(7):16–21
11. Chen CK, Lin RY (2011) A study of manufacturing models for ball-end type rotating cutters with constant pitch helical grooves. Int J Adv Manuf Technol 18:157–167
12. Lin SW, Lai HY (2001) A mathematical model for manufacturing ball-end cutters using a two-axis NC machine. Int J Adv Manuf Technol 17(12):881–888. doi:10.1007/s001700170099
13. Chen WF (2004) A mathematical solution to the design and manufacturing problems of ball-end cutters having a cutting edge with constant angle to the axis. Proc Inst Mech Eng C J Mech Eng Sci 218(3):301–308. doi:10.1243/095440604322900426

14. Tsai Y-C, Hsieh J-M (2001) A study of a design and NC manufacturing model of ball-end cutters. J Mater Process Technol 117(1–2):183–192. doi:10.1016/S0924-0136(01)01068-8
15. Chen C-B (2007) Discussion on the problems related to NC machining of toroid-shaped taper cutter with constant angle between cutting edge and the cutter axis. Int J Adv Manuf Technol 35(5–6): 493–504. doi:10.1007/s00170-006-0725-x
16. Chen WF, Lai HY, Chen CK (2001) A precision tool model for concave cone-end milling cutters. Int J Adv Manuf Technol 18(8): 567–578. doi:10.1007/s001700170033
17. Feng X, Hongzan B (2003) CNC rake grinding for a taper ball-end mill with a torus-shaped grinding wheel. Int J Adv Manuf Technol 21(8):549–555. doi:10.1007/s00170-002-1298-y
18. Pham T, Ko S (2010) A manufacturing model of an end mill using a five-axis CNC grinding machine. Int J Adv Manuf Technol 48(5–8):461–472. doi:10.1007/s00170-009-2318-y
19. Rababah M, Almagableh A, Aljarrah M (2013) Five-axis rake face grinding of end-mills with circular-arc generators. Int J Interact Des Manuf (IJIDeM):1–9. doi:10.1007/s12008-013-0198-8
20. Karpuschewski B, Jandecka K, Mourek D (2011) Automatic search for wheel position in flute grinding of cutting tools. CIRP Ann Manuf Technol 60(1):347–350. doi:10.1016/j.cirp.2011.03.113
21. Chen F, Bin H (2009) A novel CNC grinding method for the rake face of a taper ball-end mill with a CBN spherical grinding wheel. Int J Adv Manuf Technol 41(9–10):846–857. doi:10.1007/s00170-008-1554-x
22. Chen J-Y, Lee B-Y, Chen C-H (2008) Planning and analysis of grinding processes for end mills of cemented tungsten carbide. J Mater Process Technol 201(1–3):618–622. doi:10.1016/j.jmatprotec.2007.11.214
23. Kim JH, Park JW, Ko TJ (2008) End mill design and machining via cutting simulation. Comput Aided Des 40(3):324–333. doi:10.1016/j.cad.2007.11.005
24. Chen F, Hu S, Yin S (2012) A novel mathematical model for grinding ball-end milling cutter with equal rake and clearance angle. Int J Adv Manuf Technol 63(1–4):109–116. doi:10.1007/s00170-011-3889-y
25. Nguyen H, Ko S-L (2014) A mathematical model for simulating and manufacturing ball end mill. Comput Aided Des 50:16–26. doi:10.1016/j.cad.2014.01.002
26. Li G, Sun J, Li J (2014) Modeling and analysis of helical groove grinding in end mill machining. J Mater Process Technol 214(12): 3067–3076. doi:10.1016/j.jmatprotec.2014.07.009
27. Lu Y, Takeuchi Y, Takahashi I, Anzai M (2005) An integrated system development for ball end mill design, creation and evaluation. Int J Adv Manuf Technol 25(7–8):628–646. doi:10.1007/s00170-004-2259-4
28. Ji W, Liu X, Wang L, Meng Y, Wu X (2015) A study on geometry modelling of a ball-end mill with chamfered cutting edge. J Manuf Process 19:205–211. doi:10.1016/j.jmapro.2014.10.003
29. Zhou Y, Liu Y (2012) Error analysis for the non-circular curve discretization method in CNC machining. Mech Res Appl 4:54–56